


## Dual-Band Omnidirectional Invisibility of a Thin Slab with Antiscattering Coatings on Both Sides

Zhengjie Huang,<sup>1</sup> Liang Peng,<sup>2,†</sup> Zhongbo Zhu,<sup>3</sup> Xiaojun Hu,<sup>1</sup> Chun Wang,<sup>1</sup> Jingxin Tang,<sup>1</sup> and Dexin Ye<sup>1,\*</sup>

<sup>1</sup>Laboratory of Applied Research on Electromagnetics, Zhejiang University, Hangzhou 310027, China

<sup>2</sup>School of Information and Electrical Engineering, Hangzhou City University, Hangzhou 310015, China

<sup>3</sup>National Key Laboratory of Science and Technology on Space Microwave, Xi'an 710100, China

 (Received 30 August 2022; revised 22 November 2022; accepted 23 December 2022; published 9 February 2023)

Making an object invisible means that an incident electromagnetic wave is not scattered with the object being present, which has been widely studied over the past few decades. Nevertheless, rendering omnidirectional invisibility for a large object in free space is still challenging. Here, we present a dual-band antiscattering coating using a double-layered metamaterial. By putting such coatings on both sides of a thin dielectric slab, omnidirectional invisibility is observed. It is shown that the peculiar double-layered metamaterial can provide electric polarization neutralization to the original thin slab, and the Maxwell Garnett mixing rule is safely invoked to guarantee the full elimination of scattering regardless of the incident angle. Full-wave simulations and experimental measurements exhibit that a composite made of a dielectric slab sandwiched by two antiscattering coatings can avoid any scattering in both the C and Ku bands with arbitrary incident angles. The proposed approach is quite simple and nondestructive to the original objects, which can be conveniently scaled to other scenarios including terahertz and optical applications, for boosting various internet of things devices, radar radomes, noninterference isolators in optics, and invisibility cloaks.

DOI: [10.1103/PhysRevApplied.19.024028](https://doi.org/10.1103/PhysRevApplied.19.024028)

### I. INTRODUCTION

In electromagnetics, perfect invisibility means an incident electromagnetic (EM) wave is not scattered and/or disturbed with the object being present. Pioneering works indicate that invisibility may be realized through external cloaking structures designed by transformation optics [1,2]. Unfortunately, ideal invisibility cloaks require inhomogeneous and anisotropic material profiles, which are elusive to realize in practical scenarios. If the wave incidence does not show arbitrariness, e.g.,  $k$  is limited in some special directions (which is true in some practical scenarios), the realization of invisibility can be further simplified. For instance, a planar dielectric slab can be made invisible to normal incidence, as its reflection can be canceled by covering some antireflection layers [3–14]. However, conventionally designed antireflection structures do not exhibit omnidirectional invisibility, due to their limited incident angles and the phase delay involved, which strongly influences their practical applications in EM engineering including conformal stealth, antenna radomes, low-reflection sheets, etc. It is really meaningful if planar

slabs can be made scattering free, to meet the requirements in practical applications [15–17].

In principle, an individual object can be made invisible by compensating the majority of its scattering through some additional structures. For instance, carefully designed plasmonic shells can cancel the main scattering modes of objects with canonical shapes (spheres, cylinders, or cuboids), and hence a composite structure can behave as nearly invisible in free space [18–25]. This approach is of particular interest to electrically small objects. However, it can hardly work for electrically large objects, as the complex scattering modes can hardly be totally compensated.

From classical electromagnetics, a bulk material can behave as omnidirectionally invisible in free space, provided that the permittivity and permeability of its constituents are identical to those of the background medium. For instance, in Ref. [26], it is demonstrated that a designed metallic mesh structure can be made totally invisible by itself. Nevertheless, such a structure is made of electrically small building blocks, and electrically large structures can hardly be hidden inside.

In this paper, we propose an approach to make an existing slab structure (whose thickness is electrically small) invisible. Our strategy is to neutralize the polarization

\*pengl@zucc.edu.cn

†desy@zju.edu.cn

and/or magnetization of the dielectric slab with designed coatings, and the macroscopic EM behavior is reasonably interpreted through the classical Maxwell Garnett principle. In the design, an antiscattering coating is made by combining two I-shaped resonators, which can work in a couple of radar bands. By putting such metamaterial coatings on both sides of a thin dielectric slab, the electric dipole moment (the magnetic dipole moment) induced on the slab is neutralized, due to the antiphase electric polarization (magnetization) generated. On the whole, a composite made of a coating-slab-coating sandwich has effective permittivity and permeability identical to those of air, and thus it is immune to scattering in free space. Full-wave simulations are consistent with the experimental results, verifying our findings.

## II. THEORETICAL ANALYSIS

When an EM wave impinges on a thin homogeneous dielectric slab from free space, reflection and refraction generally occur, as shown in the left-hand panel of Fig. 1(a). They usually disturb the propagation of EM waves, and thus scattering is observed. The scattering can be equivalently treated as the radiation of electric dipole moment induced on the slab. Assume the relative permittivity of the dielectric slab is  $\epsilon_{r\_slab}$  ( $\epsilon_{r\_slab} > 1$ ), and the induced electric dipole moment can be approximately described as  $P_e = \int (\epsilon_{r\_slab} - 1) E dV$ , which lies in the direction identical to that of the exciting electric field  $E$ . Here,  $V$  denotes the volume occupied by the slab. Thus, the slab produces scattered fields due to the induced positive electric dipole moment. Apparently, an effective way to suppress the unwanted scattering effect is to make  $P_e$  null, i.e., zero net distribution of the electric dipole moment. Thus, additional low- (or negative-) permittivity constituents are essential to compensate the positive electric polarization.

We assume that two identical thin low-permittivity nonmagnetic coatings ( $\epsilon_{r\_coating} < 1$ ) are symmetrically attached on both sides of the dielectric slab, as depicted in the right-hand panel of Fig. 1(a). It should be noted that the spatial symmetrical distribution of coatings is to decrease the unwanted bianisotropic effect [27]. According to the EM mixing principle [28], the total electric dipole moment induced can be approximately expressed as

$$P_{e\_total} = \int (\epsilon_{r\_slab} - 1) E dV_1 + \int (\epsilon_{r\_coating} - 1) E dV_2, \quad (1)$$

where  $V_1$  and  $V_2$  are the volumes occupied by the slab and two coatings, respectively. Supposing  $P_{e\_total}$  is zero, the scattering is canceled and the whole structure is invisible in free space. Note that both the slab and coating should be electrically thin to ensure that high-order electric moments are negligible.

To give a quantitative analysis, we calculate the numerical requirements of the coating in terms of material parameters and physical volume. Assuming that the thickness of the dielectric slab is  $d_{slab}$ , then the permittivity  $\epsilon_{r\_coating}$  and thickness  $d_{coating}$  of the coatings should satisfy  $(\epsilon_{r\_slab} - 1)d_{slab} = 2(1 - \epsilon_{r\_coating})d_{coating}$ . This equation can guarantee that the effective constitutive parameters of the whole sandwich structure are the same as those of air in the quasistatic limit according to the Maxwell Garnett mixing principle [29]. Consequently, nearly perfect invisibility can be realized in free space.

As an example, by setting  $\epsilon_{r\_slab} = 3$ ,  $d_{slab} = \lambda/20$ , and  $d_{coating} = \lambda/300$ , we derive the corresponding permittivity of the antiscattering coating with  $\epsilon_{r\_coating} = -14$ . The analytically calculated transmittance amplitude and phase of the coated slab are depicted in green, as shown in Fig. 1(b). For comparison, we also plot the results for a single dielectric slab (black lines) and an air space (red dashed lines) with identical thickness to the coated slab. We can see that the single dielectric slab shows obvious impedance mismatching and phase distortion that depend on the incident angle. However, the coated slab exhibits a similar transmission response to air in both amplitude and phase for most incident angles, but with a small difference in the phase for large angles. This is because Eq. (1) is strictly valid only in the quasistatic limit. Consequently, we optimize the permittivity of the coating around  $-14$  and obtain the optimum value with  $\epsilon_{r\_coating} = -14.3$ . The corresponding transmittance amplitude and phase are denoted by the blue dashed lines. In such a case, the transmittance amplitudes are all larger than 0.999 and the maximum phase difference from air is only 0.0087 rad for incident angles ranging from  $0^\circ$  to  $88^\circ$ . This result indicates the scattering-less profile of the structure. Nevertheless, it should be noted that the thickness of the whole structure is strictly limited, to minimize the unwanted spatial dispersion and render omnidirectional invisibility. According to our calculation and simulation, the typical thickness of the whole structure can be one-fifteenth free space wavelength, for a single slab.

To directly illustrate such a performance, we simulate the electric field distributions while placing a discrete line source in front of the slab, where various incident waves are involved. Figure 1(c) shows the electric field amplitude distributions around the dielectric slab without (top panel) and with (bottom panel) two antiscattering coatings. As expected, a strong standing wave effect is observed for the single dielectric slab, while no observable scattering is seen for the coated one, showing nearly perfect invisibility.

According to the previous discussions, it is simply concluded that low- or negative-permittivity nonmagnetic materials, such as plasmonic media or metamaterials, are essential to render omnidirectional invisibility to a subwavelength-thick dielectric slab. In the following, we present a way to design an antiscattering coating based

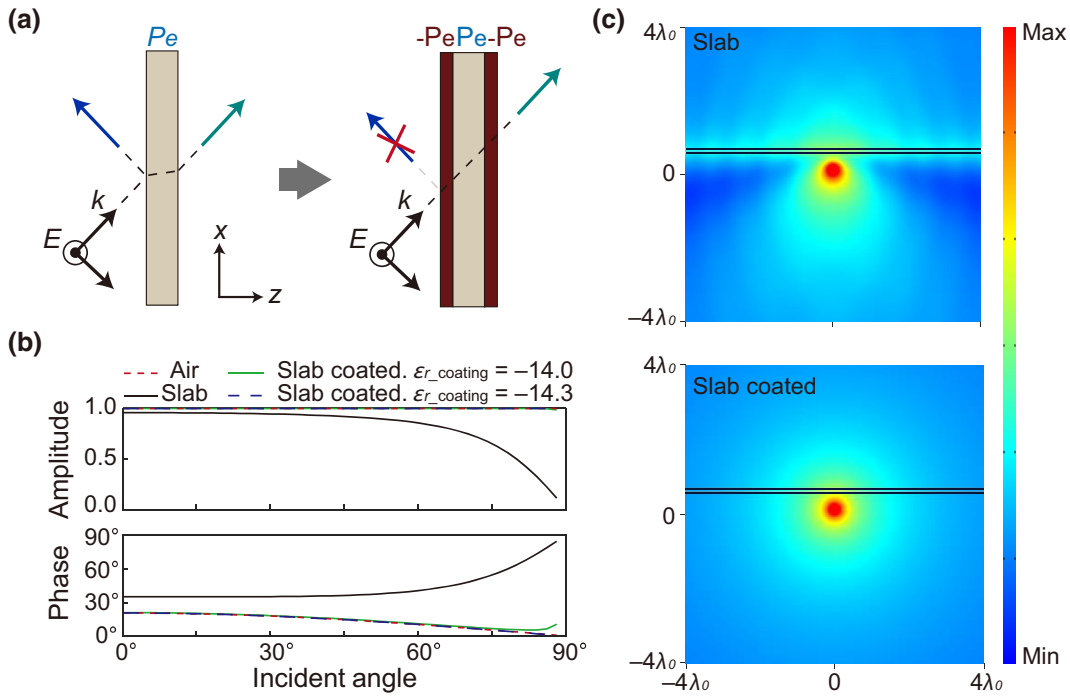


FIG. 1. Theoretical analysis. (a) Schematic diagram for rendering omnidirectional invisibility to a thin dielectric slab based on electric polarization neutralization. (b) Analytically calculated transmittance amplitude and phase of the dielectric slab without and with two negative-permittivity coatings, and an air space with identical thickness to the coated slab. (c) Simulated electric field distributions when a line source is placed in front of the dielectric slab (top panel) and the slab coated by two coatings with  $\epsilon_{r\_coating} = -14.3$  (bottom panel).

on metamaterials, which supports full polarization neutralization of a dielectric slab in two frequency bands simultaneously.

### III. DESIGN AND SIMULATION

In the material design, we introduce a metallic I-shaped resonator array to implement the antiscattering coating for transverse electric (TE) wave incidence. The I-shaped resonator has been widely used in realizing negative-permittivity metamaterials [30]. Here, to obtain a dual-band antiscattering coating, we deliberately modify the I-shaped resonator by introducing an additional pair of arms that are rolled up to obtain dual-band resonance, as shown in the bottom left-hand panel of Fig. 2(a). Then, two individual electric resonances can be manipulated by changing the length of either of the short and long metallic branches. It should be noted that due to the presence of magnetoelectric coupling, the effective permeability of the I-shaped resonator array is affected and its real part commonly exceeds unity around the resonance frequency [31]. To compensate for this effect, extra elements should be introduced to neutralize the unwanted paramagnetic response. We thus bring a closed metallic ring (CMR) structure into the unit cell, as shown in the bottom

right-hand panel of Fig. 2(a). In such a case, the macroscopic magnetic response is neutralized by the CMR's diamagnetic response [32].

The final unit cell of the coating-slab-coating sandwich structure is shown in the top panel of Fig. 2(a), where two orthogonally oriented modified I-shaped resonators are printed on a thin dielectric substrate. Five square CMRs are printed on the other side of the dielectric substrate. For two-band applications, the bigger loop is mainly designed for the lower band, and the smaller four loops are set for the higher-frequency band. The middle target dielectric slab to be compensated is assumed to be made of fiberglass material with a relative permittivity of  $\epsilon_r = 3.3$ , which is widely used in radar radome design. The thickness of the target slab is  $m = 3$  mm. For convenience, the coating dielectric substrates are set to be fiberglass, but with a thickness of  $t = 1$  mm.

We use CST Microwave Studio to perform full-wave simulations. In the simulation, periodic boundaries are used in the  $x$  and  $y$  directions, so that an infinitely large slab is implied. The incident electric field is polarized along the  $y$  axis. The metallic structures are assumed to be made of a perfect electric conductor with a thickness of 0.035 mm. For the rest of the parameters, we have  $h = 7.3$  mm,  $q = 0.2$  mm,  $k = 0.2$  mm,  $d = 0.24$  mm,  $w = 0.42$  mm,  $b = 1.7$  mm,  $o = 0.24$  mm, and  $v = 0.15$  mm,

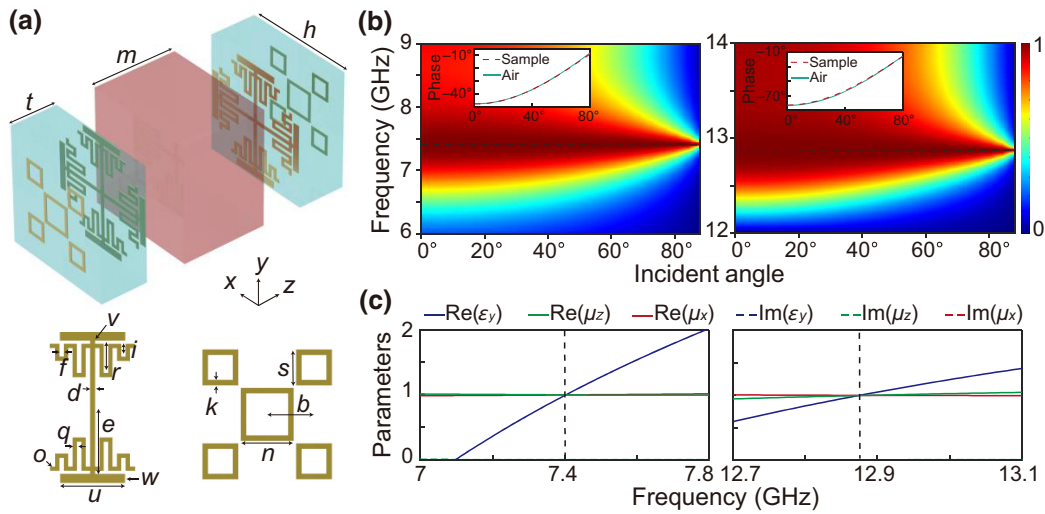


FIG. 2. Design of the antiscattering coating. (a) Unit cell of the coating-slab-coating sandwich structure. The red part denotes the middle target dielectric slab, and the two blue parts denote the coating dielectric substrates. Bottom two panels show the modified I-shaped resonator and five square CMRs printed on both sides of the coating dielectric substrates. (b) Simulated transmittance amplitudes in two frequency bands. The insets show the transmittance phases of the sandwich structure and air space with identical thickness at 7.4 GHz (left panel), and at 12.87 GHz (right panel). (c) Retrieved effective relative permittivity and permeability of the sandwich structure.

and some other geometric dimensions are optimized to be  $r = 1.35$  mm,  $i = 0.6$  mm,  $u = 3$  mm,  $n = 1.94$  mm,  $e = 3.1$  mm, and  $s = 1.3$  mm. With these parameters, full polarization neutralization can be achieved in both the C and Ku radar bands, as shown below.

Figure 2(b) shows the simulated transmittance spectra with respect to the incident angle. As can be seen, the two operating frequencies are around 7.4 GHz (C band) and 12.87 GHz (Ku band). At both frequencies, the transmittance remains almost unity for incident angles

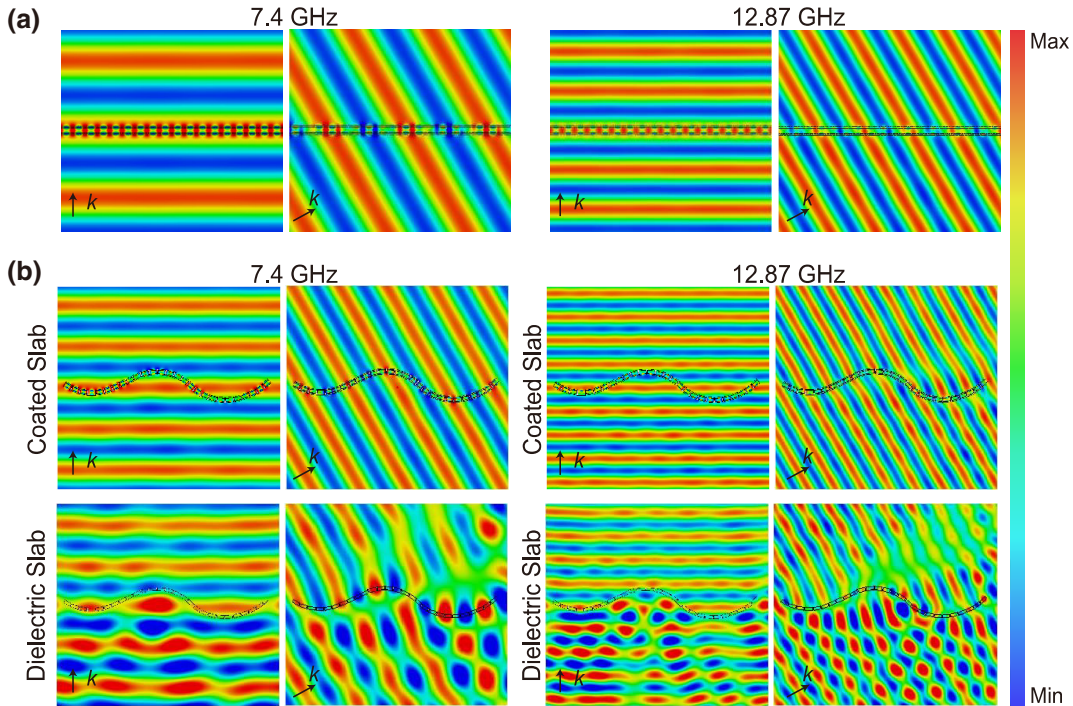


FIG. 3. Full-wave simulations. (a) Simulated electric field distributions around the planar coated slabs for  $0^\circ$  and  $60^\circ$  TE plane wave incidences at 7.4 and 12.87 GHz. (b) Simulated electric field distributions around the bent dielectric slabs with (top four panels) and without (bottom four panels) antiscattering coatings.



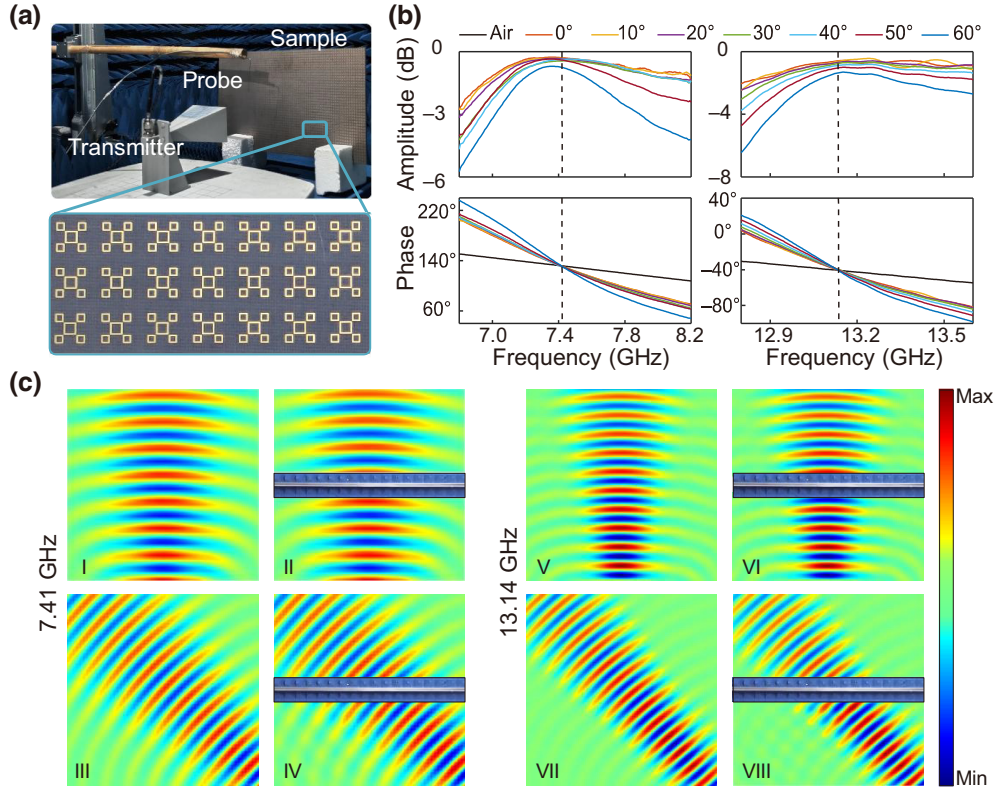


FIG. 4. Experimental measurements. (a) Photograph of the fabricated planar sample and the experimental setup. (b) Measured transmittance amplitudes and phases of the fabricated sample dependent on frequencies and incident angles. The black lines in bottom two panels denote the measured transmittance phases with the sample removed. (c) Measured electric field distributions at 7.41 GHz (four left-hand panels) and 13.14 GHz (four right-hand panels) when the radiating waves from the transmitting antenna are incident on the sample at  $0^\circ$  (panels II and VI) and  $45^\circ$  (panels IV and VIII). Panels I, III, V, and VII show the corresponding results measured with the sample removed.

ranging from  $0^\circ$  to  $88^\circ$ , exhibiting nearly omnidirectional impedance matching. More importantly, the phase of transmittance coincides with that of air with identical thickness, for all the incident angles. As shown in the two inserts of Fig. 2(b), the maximum phase differences are only 0.0176 rad at 7.4 GHz and 0.0246 rad at 12.87 GHz for this 5-mm-thick composite slab.

Previous results show that the coated slab exhibits an airlike EM response. Macroscopically, it should have the same constitutive parameters as air. Since the total thickness is kept less than  $1/4$  wavelength at both operating frequencies, the overall EM characteristics of the sandwich structure can be described with effective parameters. We thus retrieve the effective parameters of the sandwich structure in three directions, by applying the retrieval approach [33], and the results are shown in Fig. 2(c). It is seen that  $\epsilon_y = \mu_x = \mu_z \approx 0.997$  at 7.4 GHz, while  $\epsilon_y = \mu_x = \mu_z \approx 0.996$  at 12.87 GHz, showing airlike property and agreeing well with our analysis.

As a direct illustration of the omnidirectional invisibility, we draw the electric field distributions around the planar composite slab for different incident angles ( $0^\circ$  and

$60^\circ$ ) at two operating frequencies, as shown in Fig. 3(a). It is seen that the electric fields are almost undisturbed as the composite slab is not seen by the incident plane waves, showing perfect omnidirectional invisibility.

Considering that the polarization neutralization is implemented at a subwavelength scale, the slight deformation might have no obvious influence on the holistic characteristics. To validate this, we perform full-wave simulations with bending of the slab structure. As shown in Fig. 3(b), the incident plane waves are almost undisturbed if the target slab is covered with the antiscattering coatings (top four panels), but strong scattering is excited if the antiscattering coating is not present (bottom four panels). All the results imply that the proposed antiscattering coating is effective for both planar and bent dielectric slabs, which enables potential implementation in practical applications.

#### IV. EXPERIMENT AND DISCUSSION

In the experiments, we fabricate a planar sample using printed circuit board lithography. The overall dimensions of the sample are  $550 \times 300 \times 5.4 \text{ mm}^3$

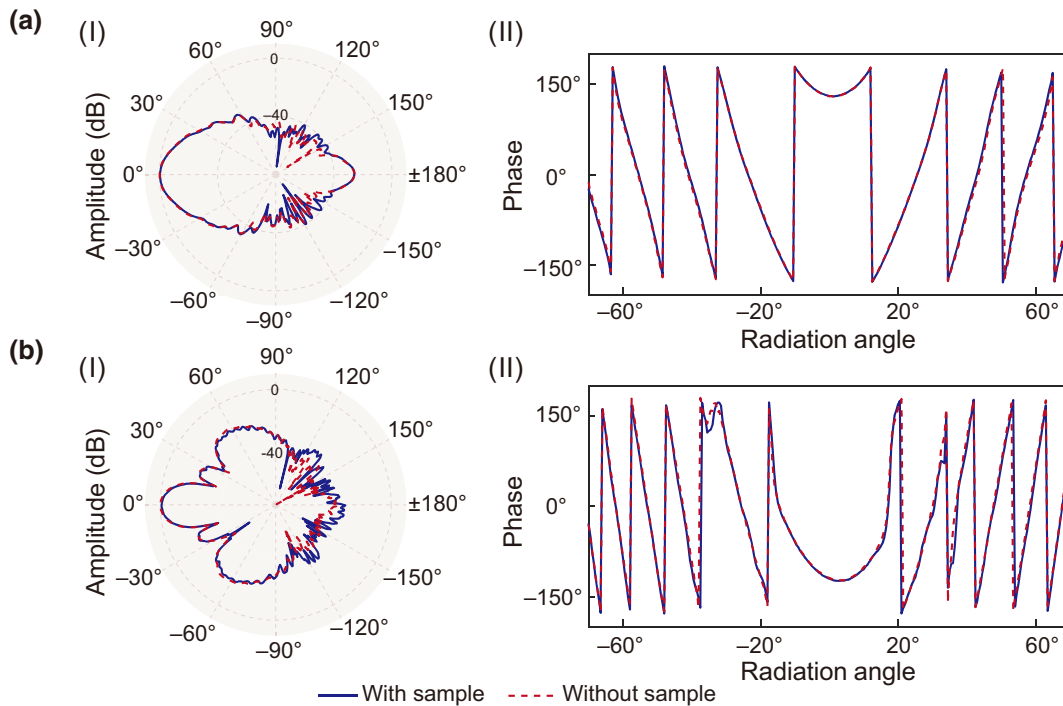


FIG. 5. Measured far-field radiation patterns (I) and phases (II) at (a) 7.41 GHz and (b) 13.14 GHz. The blue lines show the results when the fabricated sample is placed in front of the transmitting horn antenna and the red dashed lines show the results with the sample removed.

( $75 \times 41 \times 1$  units<sup>3</sup>), as shown in Fig. 4(a). All geometric dimensions of each unit are the same as those used in the simulations.

First, the transmission performance is characterized in an anechoic chamber using an Agilent 8722ES network analyzer and two pairs of horn antennas, operating in the C and Ku bands, respectively. In the measurements, two identical antennas are placed face to face with a distance of 1.5 m, and the planar sample is placed in the center of the two antennas. The spatial orientation of the planar sample is controlled by the supporting stage, and the incident angle is changed by rotating the stage. Figure 4(b) shows the measured transmittance amplitudes (top panels) and phases (bottom panels), with varying the incident angles. The transmittance amplitudes are normalized by those with the sample removed. We can see that the maximum amplitudes appear around 7.41 GHz in the C band and 13.14 GHz in the Ku band. At 7.41 GHz, the transmittance amplitudes are all larger than  $-0.74$  dB for incident angles ranging from  $0^\circ$  to  $60^\circ$ , and larger than  $-1.35$  dB at 13.14 GHz. Meanwhile, the transmittance phases at the two operating frequencies are nearly the same as those measured with the sample removed, as shown in the bottom panels of Fig. 4(b). The maximum phase differences are 0.0164 rad at 7.41 GHz and 0.0122 rad at 13.14 GHz. All the results imply that the incident waves stay nearly undisturbed in both amplitude and phase while passing through the planar sample with varying the incident angles.

Concerning the larger deviation for the higher operating frequency, the reasons could be twofold. First, the EM response of the resonator is influenced by fabrication errors. The high-frequency EM performance is somewhat more sensitive to the dimensions of the metallic structures than the low-frequency performance, due to the reduced wavelength. Second, material imperfections may also lead to frequency shifting. In the simulations, the substrate’s permittivity is an ideal and nondispersive parameter. In contrast, the practical substrate may not have exactly identical permittivity in the C and Ku bands, which leads to the shift in the oscillating frequency of the structure.

For better interpretation, we measure the electric field distributions when the radiating waves from the transmitting antenna are incident on the sample at  $0^\circ$  (panels II and VI) and  $45^\circ$  (panels IV and VIII), as shown in Fig. 4(c). In the measurement, the spatial step resolutions are 6 mm for 7.41 GHz and 3 mm for 13.14 GHz. For comparison, the electric field distributions with the sample removed are also recorded, as shown in panels I, III, V, and VII. With all the figures, we note that it is evident that the composite slab exhibits an airlike EM property regardless of the incident angle, which validates the simulated results shown in Fig. 3(a).

Finally, we characterize the performance of the fabricated sample in an antenna radome scenario. In the measurement, the fabricated sample is placed 5 cm away from the transmitting horn antenna, and the far-field

radiation is measured by another identical antenna 4.6 m away from the transmitting one. The blue lines in Figs. 5(a) and 5(b) show the measured amplitudes (panel I) and phases (panel II) at 7.41 and 13.14 GHz, respectively. For comparison, the red dashed lines show the results with the sample removed. We can see that two far-field radiations are nearly identical in both amplitude and phase, in the forward-radiating range from  $-70^\circ$  to  $70^\circ$ . The fabricated sample performs as a wide-angle (almost omnidirectional) invisibility slab at the two operating frequencies.

## V. CONCLUSION

In conclusion, we demonstrate an approach to render omnidirectional invisibility to thin dielectric slabs. The key concept is the introduction of an antiscattering coating with an antiphase electric dipole moment, which provides purely electric polarization neutralization to the original thin slab, and thus eliminates the scattering effect, regardless of the incident angle. As a proof of concept, we design a particular antiscattering coating by using a double-layered metamaterial. Full-wave simulations and experimental measurements show that the sandwich structure composed of a dielectric slab and two antiscattering coatings is omnidirectionally invisible under TE wave incidence at both the C and Ku bands. Although in our current design we only focus on the TE polarization incidence, and all the structures are designed and optimized to match the TE polarization, the proposed polarization and/or magnetization neutralization concept is applicable for both TE and TM waves due to their duality characteristics. Under TM wave incidence, the permittivity of the antiscattering coating should be anisotropic in the normal and tangential directions according to the Maxwell Garnett mixing principle. The proposed approach is simple, robust, and nondestructive to the original dielectric objects, which can be conveniently scaled to any other scenarios, including terahertz and optical applications.

## ACKNOWLEDGMENTS

This work is supported by the National Natural Science Foundation of China (NSFC) under Grants No. 62122068, No. 62071420, No. 62271439, and No. 61875051 and the Natural Science Foundation of Zhejiang Province (ZJNSF) under Grant No. LR21F010002.

## AUTHOR CONTRIBUTIONS

Z.H., L.P., D.Y. designed the research; Z.H., L.P., Z.Z., X.H., C.W., J.T., D.Y. performed the research. All authors contributed to data interpretation and the composition of the manuscript.

- [1] J. B. Pendry, D. Schurig, and D. R. Smith, Controlling electromagnetic fields, *Science* **312**, 1780 (2006).
- [2] D. Schurig, J. J. Mock, B. J. Justice, S. A. Cummer, J. B. Pendry, A. F. Starr, and D. R. Smith, Metamaterial electromagnetic cloak at microwave frequencies, *Science* **314**, 977 (2006).
- [3] W. H. Southwell, Gradient-index anti-reflection coatings, *Opt. Lett.* **8**, 584 (1983).
- [4] H. Chen, J. Zhou, J. F. O'Hara, F. Chen, A. K. Azad, and A. J. Taylor, Antireflection Coating Using Metamaterials and Identification of Its Mechanism, *Phys. Rev. Lett.* **105**, 073901 (2010).
- [5] S. Chhajed, D. J. Poxson, X. Yan, J. Cho, E. F. Schubert, R. E. Welsler, A. K. Sood, and J. K. Kim, Nanostructured multilayer tailored-refractive-index antireflection coating for glass with broadband and omnidirectional characteristics, *Appl. Phys. Express* **4**, 052503 (2011).
- [6] J. Sun, L. Liu, G. Dong, and J. Zhou, An extremely broad band metamaterial absorber based on destructive interference, *Opt. Express* **19**, 21155 (2011).
- [7] B. Zhang, J. Hendrickson, N. Nader, H. Chen, and J. Guo, Metasurface optical antireflection coating, *Appl. Phys. Lett.* **105**, 241113 (2014).
- [8] S. V. Boriskina, Making invisible materials, *Nat. Photonics* **9**, 422 (2015).
- [9] L. Huang, C. Chang, B. Zeng, J. Nogan, S. Luo, A. J. Taylor, A. K. Azad, and H. Chen, Bilayer metasurfaces for dual- and broadband optical antireflection, *ACS Photonics* **4**, 2111 (2017).
- [10] T. Hao, W. Zheng, W. Wang, Y. Zhou, J. Bai, K. Lin, and Z. Yu, Electrically thin metasurface for broadband transmission enhancement by manipulating the amplitude and phase of the reflection coefficients, *J. Appl. Phys.* **126**, 025303 (2019).
- [11] K. W. Allen, D. J. P. Dykes, D. R. Reid, and R. T. Lee, Multi-objective genetic algorithm optimization of frequency selective metasurfaces to engineer ku-passband filter responses, *Prog. Electromagn. Res.* **167**, 19 (2020).
- [12] F. Yang, B. O. Raeker, D. T. Nguyen, J. D. Miller, Z. Xiong, A. Grbic, and J. S. Ho, Antireflection and Wavefront Manipulation with Cascaded Metasurfaces, *Phys. Rev. Appl.* **14**, 064044 (2020).
- [13] H. Chu, H. Zhang, Y. Zhang, R. Peng, M. Wang, Y. Hao, and Y. Lai, Invisible surfaces enabled by the coalescence of anti-reflection and wavefront controllability in ultrathin metasurfaces, *Nat. Commun.* **12**, 4523 (2021).
- [14] S. Sajuyigbe, B. J. Justice, A. F. Starr, and D. R. Smith, Design and analysis of three-dimensionalized elc metamaterial unit cell, *IEEE Antennas Wirel. Propag. Lett.* **8**, 1268 (2009).
- [15] V. Kuhn, C. Lahuec, F. Seguin, and C. Person, A multi-band stacked RF energy harvester with RF-to-dc efficiency up to 84%, *IEEE Trans. Microwave Theory Tech.* **63**, 1768 (2015).
- [16] Y. Li, C. Y. Sim, Y. Luo, and G. Yang, Multiband 10-antenna array for sub-6 GHz mimo applications in 5-g smartphones, *IEEE Access* **6**, 28041 (2018).
- [17] X. Wang, X. Wang, H. Ren, N. Wu, J. Wu, W. Su, Y. Han, and S. Xu, Optically transparent microwave shielding hybrid film composited by metal mesh and graphene, *Prog. Electromagn. Res.* **170**, 187 (2021).

- [18] A. Alu and N. Engheta, Achieving transparency with plasmonic and metamaterial coatings, *Phys. Rev. E* **72**, 016623 (2005).
- [19] E. Irci and V. B. Erturk, Achieving transparency and maximizing scattering with metamaterial-coated conducting cylinders, *Phys. Rev. E* **76**, 056603 (2007).
- [20] B. Edwards, A. Alu, M. G. Silveirinha, and N. Engheta, Experimental Verification of Plasmonic Cloaking at Microwave Frequencies with Metamaterials, *Phys. Rev. Lett.* **103**, 153901 (2009).
- [21] A. Monti, J. C. Soric, A. Alu, A. Toscano, and F. Bilotti, Anisotropic mantle cloaks for TM and TE scattering reduction, *IEEE Trans. Antennas Propag.* **63**, 1775 (2015).
- [22] A. S. Shalin, P. Ginzburg, A. A. Orlov, I. Iorsh, P. A. Belov, Y. S. Kivshar, and A. V. Zayats, Scattering suppression from arbitrary objects in spatially dispersive layered metamaterials, *Phys. Rev. B* **91**, 125426 (2015).
- [23] H. Younesiraad, M. Bemani, and S. Nikmehr, Scattering suppression and cloak for electrically large objects using cylindrical metasurface based on monolayer and multilayer mantle cloak approach, *IET Microwave Antennas Propag.* **13**, 278 (2019).
- [24] C. Wang, C. Qian, H. Hu, L. Shen, Z. Wang, H. Wang, Z. Xu, B. Zhang, H. Chen, & X. Lin, Superscattering of light in refractive-index near-zero environments, *Prog. Electromagn. Res.* **168**, 15 (2020).
- [25] K. Zheng, Z. Zhang, F. Qin, and Y. Xu, Invisible Mie scatterer, *Opt. Lett.* **46**, 5248 (2021).
- [26] D. Ye, L. Lu, J. D. Joannopoulos, M. Soljacic, and L. Ran, Invisible metallic mesh, *Proc. Natl. Acad. Sci. U. S. A.* **113**, 2568 (2016).
- [27] D. R. Smith, J. Gollub, J. J. Mock, W. J. Padilla, and D. Schurig, Calculation and measurement of bianisotropy in a split ring resonator metamaterial, *J. Appl. Phys.* **100**, 024507 (2006).
- [28] A. H. Sihvola, *Electromagnetic Mixing Formulas and Applications* (Institution of Electrical Engineers, London, UK, 1999).
- [29] D. J. Bergman, Dielectric constant of a composite material: A problem in classical physics, *Phys. Rep.* **43**, 378 (1978).
- [30] D. Ye, K. H. Chang, L. Ran, and H. Xin, Microwave gain medium with negative refractive index, *Nat. Commun.* **5**, 5841 (2014).
- [31] A. Alu, Restoring the physical meaning of metamaterial constitutive parameters, *Phys. Rev. B* **83**, 081102 (2011).
- [32] J. B. Pendry, A. J. Holden, D. J. Robbins, and W. J. Stewart, Magnetism from conductors and enhanced nonlinear phenomena, *IEEE Trans. Microwave Theory Tech.* **47**, 2075 (1999).
- [33] X. Chen, T. M. Grzegorzcyk, B. Wu, J. Pacheco, and J. A. Kong, Robust method to retrieve the constitutive effective parameters of metamaterials, *Phys. Rev. E* **70**, 016608 (2004).